Pressure-Induced Superconductivity up to 9 K in the Quasi-One-Dimensional KMn_6Bi_5

Z. Y. Liu,[1,2,*] Q. X. Dong,[1,2,*] P. T. Yang,[1,2,*] P. F. Shan,[1,2] B. S. Wang,[1,2,†] J. P. Sun,[1,2] Z. L. Dun,[1,2] Y. Uwatoko,[3] G. F. Chen,[1,2,‡] X. L. Dong,[1,2] Z. X. Zhao,[1,2] and J.-G. Cheng[1,2,§]

[1]*Beijing National Laboratory for Condensed Matter Physics and Institute of Physics, Chinese Academy of Sciences, Beijing 100190, China*

[2]*School of Physical Sciences, University of Chinese Academy of Sciences, Beijing 100190, China*

[3]*Institute for Solid State Physics, University of Tokyo, Kashiwa, Chiba 277-8581, Japan*

(Received 20 January 2022; revised 13 March 2022; accepted 7 April 2022; published 4 May 2022)

The Mn-based superconductor is rare owing to the strong magnetic pair-breaking effect. Here we report on the discovery of pressure-induced superconductivity in KMn_6Bi_5, which becomes the first *ternary* Mn-based superconductor. At ambient pressure, the quasi-one-dimensional KMn_6Bi_5 is an antiferromagnetic metal with $T_N \approx 75$ K. By measuring resistance and ac magnetic susceptibility under hydrostatic pressures up to 14.2 GPa in a cubic anvil cell apparatus, we find that its antiferromagnetic transition can be suppressed completely at a critical pressure of $P_c \approx 13$ GPa, around which bulk superconductivity emerges and displays a superconducting dome with the maximal $T_c^{\text{onset}} = 9.3$ K achieved at about 14 GPa. The close proximity of superconductivity to a magnetic instability in the temperature-pressure phase diagram of KMn_6Bi_5 and an unusually large $\mu_0 H_{c2}(0)$ exceeding the Pauli paramagnetic limit suggests an unconventional magnetism-mediated paring mechanism. In contrast to the binary MnP, the flexibility of the crystal structure and chemical compositions in the ternary AMn_6Bi_5 (A = alkali metal) can open a new avenue for finding more Mn-based superconductors.

DOI: 10.1103/PhysRevLett.128.187001

Introduction.—Unconventional superconductivity beyond the Bardeen-Cooper-Schrieffer theory usually emerges on the border of long-range antiferromagnetic order as exemplified by the cuprate [1,2], iron-pnictide [3,4], and heavy-fermion superconductors [5,6]. In these cases, the enhanced magnetic fluctuations are believed to be the binding glue of Cooper pairs. As such, it is expected to find unconventional superconductivity in the vicinity of the antiferromagnetic quantum critical point (QCP), which can be achieved by employing external tuning parameters such as chemical doping and applying physical pressure [1–6]. By following this approach, we discovered the first Mn-based superconductor MnP by suppressing its helimagnetic order via the application of high pressure [7]. Its superconducting transition temperature $T_c \approx 1$ K is low and the superconductivity only appears in a narrow pressure range around $P_c \approx 8$ GPa where the helimagnetic order just vanishes. Since MnP is a three-dimensional binary compound, other tuning methods except for applying pressure are less effective in regulating its magnetism and inducing superconductivity. In this regard, it is more attractive to achieve superconductivity in the ternary or complex Mn-based compounds, especially those having low-dimensional structures in recognizing the common features of known high-T_c superconductors.

To this end, we turn our attention to a newly synthesized ternary compound KMn_6Bi_5 [8], which adopts a quasi-one-dimensional (Q1D) monoclinic structure. As illustrated in Fig. 1(a), the most prominent structural feature of this compound is the presence of infinite $[Mn_6Bi_5]^-$ columns composed of an outer nanotube of Bi atoms (diameter ~8.7 Å) surrounding an inner Mn-Mn bonded metallic core. The inner core can be described as a vertice-sharing distorted Mn-centered icosahedra along the column direction, i.e., b axis. The short interatomic Mn-Mn and Bi-Bi distances in comparable to those in the corresponding metal elements render a metallic conductivity for this compound, and the Q1D character produces a pronounced anisotropy in physical properties. Upon cooling down at ambient pressure (AP), it undergoes an antiferromagnetic transition at $T_N \approx 75$ K, which is manifested as a kink in resistivity $\rho_{//}$ along the rod but an upturn in the $\rho_\perp$ perpendicular to the rod [8]. Analyses of the paramagnetic susceptibility $\chi(T)$ above T_N in terms of the modified Curie-Weiss law yield a relatively small effective moment of Mn, i.e., $1.56\mu_B$ for $\chi_{//}$ and $1.37\mu_B$ for $\chi_\perp$, respectively, signaling an itinerant nature of the magnetism similar to MnP [7]. First-principles calculations on its sister compound $RbMn_6Bi_5$ have revealed that the density of states at the Fermi level are dominated by the Mn-3d electrons and the helical antiferromagnetic structures are stable [9]. The itinerant-electron magnetism with relatively low T_N makes KMn_6Bi_5 a potential candidate for exploring unconventional superconductivity near the magnetic QCP. In particular, the enhanced magnetic fluctuations pertinent to the strong Q1D structure are expected to promote stronger superconducting pairing and thus higher T_c in comparison to the three-dimensional MnP [7].

We thus employed a high-pressure approach to explore superconductivity in KMn_6Bi_5 single crystal by measuring its electrical transport and ac magnetic susceptibility under various pressures up to 23 GPa. We find that its antiferromagnetic order is first enhanced moderately and then suppressed completely at $P_c \approx 13$ GPa, around which bulk superconductivity emerges and exhibits a domelike $T_c(P)$ with the maximal $T_c^{\text{onset}} = 9.3$ K achieved at 14.2 GPa. The close proximity of superconductivity to a magnetic instability indicates an unconventional magnetism-mediate paring mechanism and KMn_6Bi_5 becomes the first ternary Mn-based superconductor. The present work can open a new avenue for finding more Mn-based superconductors in the ternary AMn_6Bi_5 (A = alkali metal) with flexible crystal structure and different chemical variants.

Experimental.—The KMn_6Bi_5 crystals used in the present study were grown with the self-flux method as described elsewhere [8]. The quality of the crystals was checked by single-crystal x-ray diffraction (XRD) at room temperature, and the obtained lattice parameters in the monoclinic structure ($C2/m$) are consistent with previous reports [8]. The chemical composition, K:Mn:Bi = 1:6:5, close to the stoichiometric one is verified via the energy dispersive spectroscopy measurements. Electrical transport and magnetic properties at AP were measured with the Quantum Design Physical Property Measurement System (PPMS-9T) and Magnetic Property Measurement System (MPMS-III), respectively. High-pressure resistance measured along the b axis with standard four-probe configurations up to 14.2 GPa were carried out with a palm-type cubic anvil cell (CAC), which can generate excellent hydrostatic pressures due to the three-axis compression geometry and the adoption of liquid pressure transmitting medium (PTM). ac magnetic susceptibility under pressure was also measured in CAC by mutual induction method at a fixed frequency of 317 Hz with ac magnetic field of few Oe parallel to the b axis. The primary and secondary coils are made of enameled cooper wires of 25 μm in diameter with a total of ~40 turns for each coil. The glycerol is employed as the PTM for the high-pressure measurements in CAC, and the pressure values were estimated based on the superconducting transition of Pb at low temperatures [10,11]. We also measured resistance under quasihydrostatic pressures up to 23 GPa by using a BeCu-type diamond pressure cell (DAC) with 300-μm culets. In this case, soft KBr powder was employed as the solid PTM. The pressure in DAC was determined at room temperature by the Ruby fluorescence method. All experiments were carried out in a ^{4}He refrigerated cryostat equipped with a 9 T superconducting magnet at the Synergic Extreme Condition User Facility (SECUF).

Results and discussion.—Before performing high-pressure studies, we first characterized the physical properties of KMn_6Bi_5 at AP. Figure 1(b) shows the temperature dependences of resistivity $\rho(T)$ and magnetic susceptibility

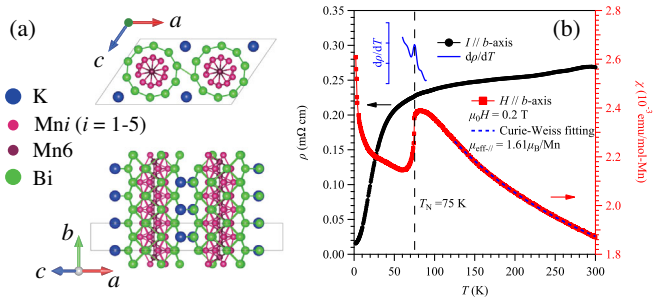

FIG. 1. (a) Crystal structure of single-crystal KMn_6Bi_5. (b) Temperature dependence of resistivity $\rho(T)$ and its derivative $d\rho/dT$ along the b axis at ambient pressure (left axis). The antiferromagnetic transition at T_N is marked by vertical broken line. Temperature dependence of magnetic susceptibility $\chi(T)$ (right axis) recorded at a magnetic field of 0.2 T. The Curie-Weiss fitting is shown by the dotted line.

$\chi(T)$ along the b axis. All results are in excellent agreement with those in the previous report [8], and consistently confirm the occurrence of an antiferromagnetic transition at $T_N \approx 75$ K, manifested as a sudden drop in $\chi(T)$, a weak kink in $\rho(T)$ and a peak in $d\rho/dT$. The residual resistivity ratio ($RRR \equiv \rho_{300\text{ K}}/\rho_{2\text{ K}}$) is ~17 in this study, comparable to ~19 in Ref. [8], further confirming the high quality of the studied KMn_6Bi_5 crystals. We noticed that $\rho(T)$ decreases quickly while $\chi(T)$ exhibits a broad hump centered at 40 K, which might be correlated with the rearrangement of Mn spins [8]. We have studied four KMn_6Bi_5 samples (#1 to #4) under high pressures and listed their dimensions in Table S1 of the Supplemental Material [12].

Figure 2(a) shows the resistance $R(T)$ of KMn_6Bi_5 (#1) under various pressures up to 14.2 GPa measured in CAC in the temperature range 1.5–300 K. With increasing pressure up to 4 GPa, the $R(T)$ and its derivative dR/dT retains similar temperature dependence and the values of T_N raise slightly up to ~86 K at 4 GPa. At $P \geq 6.2$ GPa, the kinklike feature vanishes and changes to a weak humplike anomaly, corresponding to a broad dip in dR/dT as shown in Figs. 2(b) and S1 in Ref. [12]. Noted that the humplike anomaly is very weak and we have to examine carefully $R(T)$ and dR/dT together to determine T_N as illustrated in Fig. 2(c). Such a change should be ascribed to a pressure-induced subtle modification of magnetic structure in KMn_6Bi_5, which can affect the electronic states at Fermi level and the corresponding magnetic scatterings. Similar behaviors have been recently observed in the quasi-2D kagome material CsV_3Sb_5 under pressures [13], which has been ascribed to the modification of the charge-density-wave state when the interlayer distance shrinks quickly upon compression. The strong reduction of interchain distances of Q1D KMn_6Bi_5 under pressure can influence the interchain exchange interactions and thus modify the magnetic structure, resulting in the corresponding changes of $R(T)$ around T_N. Upon further increasing pressure, the resistance anomaly at T_N is further

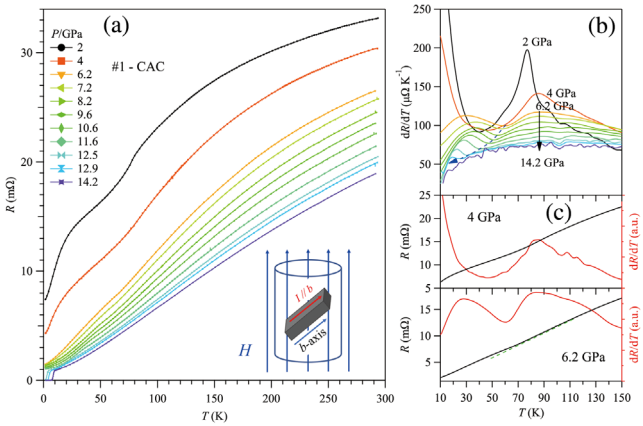

FIG. 2. (a) Electrical resistance of KMn_6Bi_5 (#1) under various hydrostatic pressures up to 14.2 GPa measured in CAC. (b) The corresponding dR/dT curves. (c) The $R(T)$ and corresponding dR/dT curves at 4 and 6.2 GPa highlighting the distinct features around T_N. Inset of (a) shows the sample configuration in CAC. The electric current (I) was applied along the b axis, while the magnetic field (H) has an angle about 45° with respect to the b axis. Noted that the angle between the H and b axis may change slightly due to the rotation or movement of the sample upon compression.

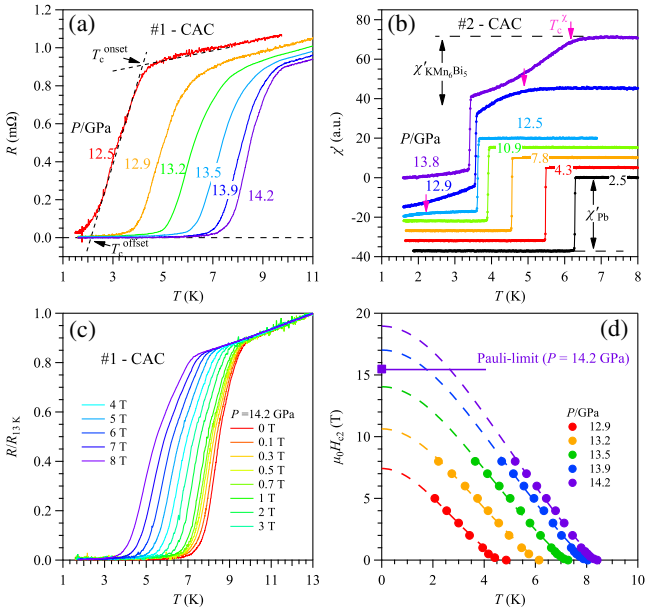

FIG. 3. (a) The enlarged view of low-T resistance data ($0 \le T \le 11$ K), in which the T_c^{onset} and T_c^{offset} are marked by arrows. (b) The ac magnetic susceptibility $4\pi\chi_{\text{ac}}(T)$ of KMn_6Bi_5 and Pb with similar volume. The arrows show the superconducting transition temperature T_c^{χ} of KMn_6Bi_5 crystal. (c) The low-temperature normalized $R/R_{13\,\text{K}}(T)$ under different fields at 14.2 GPa. (d) The temperature dependences of $\mu_0 H_{c2}(T)$ fitted by the Ginzburg-Landau (GL) equation; the Pauli limit of $\mu_0 H_p = 1.84 T_c$ at 14.2 GPa is indicated.

weakened and the corresponding T_N is lowered progressively, reaching ~25 K at 12.9 GPa, above which no anomaly can be discerned in $R(T)$. This indicates that the long-range antiferromagnetic order of KMn_6Bi_5 is completely suppressed by pressure.

Accompanied with the gradual suppression of antiferromagnetic transition by pressure, we observed a sudden drop of resistance at low temperatures above 12.5 GPa, indicating the possible occurrence of superconductivity in KMn_6Bi_5. The low-temperature $R(T)$ shown in Fig. 3(a) depicts clearly the evolution of the superconducting transition. As shown, $R(T)$ at 12.5 GPa starts to drop quickly at ~4 K but cannot reach zero down to 1.5 K. The superconducting transition moves quickly to higher temperatures with increasing pressure and zero-resistance state is realized at $P \ge 12.9$ GPa. Since the observed transition is relatively broad, here we define the onset and offset of superconducting transition, T_c^{onset} and T_c^{offset}, as the intersection points of two straight lines below and above the transition as illustrated in Fig. 3(a). At 14.2 GPa, T_c^{onset} and T_c^{offset} reach about 9.3 and 7.6 K, respectively. Noted that the increment of T_c with pressure becomes less efficient above 13.5 GPa, leading to a saturation trend of $T_c(P)$ as shown below.

To confirm the bulk nature of the superconducting state, we measured ac magnetic susceptibility $\chi_{ac}(T)$ of KMn_6Bi_5 (#2) together with a piece of Pb; the superconducting shielding volume fraction $4\pi\chi_{\text{ac}}(T)$ of KMn_6Bi_5 can be estimated by comparing its diamagnetic signal with that of Pb. As shown in Fig. 3(b), the superconducting transition of Pb is quite sharp and moves down progressively with increasing pressure, elaborating an excellent hydrostatic pressure environment in CAC. In perfect agreement with the $R(T)$ data, the superconducting transition in $\chi_{\text{ac}}(T)$ marked by T_c^{χ} starts to appear around 2.2 K at 12.5 GPa and quickly increases up to ~6 K at 13.8 GPa; accordingly, the $4\pi\chi_v(1.5\text{ K})$ increases monotonously with pressure from nearly zero at 12.5 GPa to over 90% at 13.8 GPa. From these high-pressure transport and magnetic susceptibility measurements, we can conclude that bulk superconductivity emerges in KMn_6Bi_5 around $P_c \approx 13$ GPa, where the long-range antiferromagnetic transition vanishes completely.

To see a complete evolution of superconducting state under higher pressure, we measured $R(T)$ of KMn_6Bi_5 (#3) up to 23 GPa by using a DAC. As shown in Fig. S2 [12], it enters the superconducting state with a pronounced drop in resistance as marked by T_c^{onset}, but zero resistance cannot be reached due to the nonhydrostatic pressure conditions in DAC employing solid PTM, i.e., the presence of pressure inhomogeneity and shear stress. T_c^{onset} increases monotonously from ~4.95 K at 12.1 GPa to a maximum of ~7.0 K at 14.9 GPa, and then decreases to ~3.0 K at 23.1 GPa. These results suggest the presence of a superconducting dome in KMn_6Bi_5. The difference of maximal T_c^{onset} in DAC and CAC should be ascribed to the different pressure environments of these two techniques.

To further characterize the superconducting state of KMn_6Bi_5, we measured low-temperature $R(T)$ under different magnetic fields at each pressure. All the $R(T)$ data are given in Fig. S3 [12], and the normalized data at 14.2 GPa are shown in Fig. 3(c) as a representative. The superconducting transition shifts to lower temperatures gradually with increasing magnetic fields as expected. However, the application of an 8 T field cannot eliminate the superconducting transition at 14.2 GPa, implying a high upper critical field $\mu_0 H_{c2}$. To quantify the evolution of $\mu_0 H_{c2}$, here we used the criteria of 50% R_n for T_c and plotted the temperature dependences of $\mu_0 H_{c2}(T)$ in Fig. 3(d). The experimental data can be described by the Ginzburg-Landau (GL) equation, $\mu_0 H_{c2}(T) = \mu_0 H_{c2}(0)[1-(T/T_c)^2]/[1+(T/T_c)^2]$ [14]. The best fits shown by the dashed lines in Fig. 3(d) yield zero-temperature $\mu_0 H_{c2}(0)$ values for each pressure. Accordingly, the coherence lengths $\xi(0)$ at each pressure can be obtained based on the equation $\mu_0 H_{c2}(0) = \Phi_0/2\pi\xi(0)^2$, where $\Phi_0 = h/2e$ is the magnetic flux quantum. The obtained values of $\mu_0 H_{c2}(0)$ and $\xi(0)$ under different pressures are collected in the Table S2 [12]. With increasing pressure from 12.9 to 14.2 GPa, $\mu_0 H_{c2}(0)$ increases dramatically from 7.42 to 18.95 T, while $\xi(0)$ decreases from 66.6 to 41.7 Å. It is noteworthy that the $\mu_0 H_{c2}(0)$ at 14.2 GPa exceeds the Pauli paramagnetic limit of $\mu_0 H_p = 1.84 T_c =$ 15.2 T [15], implying the presence of strong coupling effect or a possible unconventional pairing mechanism.

To ensure the reproducibility of the obtained results, we performed additional high-pressure resistance measurements on KMn_6Bi_5 (#4) in CAC up to 13.3 GPa. As shown in Figs. S4–S5 in the Supplemental Material [12], both $R(T)$ and T_N show similar pressure dependences to those of KMn_6Bi_5 (#1); T_N is extremely weak above 11 GPa and the superconducting T_c^{onset} reaches 6.5 K at 13.3 GPa. These results confirm that our findings are reliable and reproducible. After finishing all $R(T)$ measurements, we checked its $R(T)$ on releasing pressure to ~3 GPa as shown in Fig. S4 [12]. We find that superconductivity disappears completely, implying that the studied sample undergoes a reversible change under pressure. As shown in Fig. S6 [12], single-crystal XRD on sample #4 recovered after high-pressure $R(T)$ measurements further confirmed the stability of sample under pressures.

Based on the above results, we construct a temperature-pressure phase diagram of KMn_6Bi_5 as shown in the Fig. 4(a). With increasing pressure, T_N first increases slightly until 4 GPa, then shows a sudden decrease at ~6 GPa, and collapses completely at $P_c \approx 13$ GPa. The pressure dependence of $T_N(P)$ at $P \geq 6.2$ GPa can be fitted by the empirical model $T_N = T_0(1-P/P_c)^\beta$, where β represents the critical exponent. The best fitting yields $T_0 = 70.7$ K, $P_c = 13.1$ GPa, and $\beta = 0.25$, respectively. Bulk superconductivity emerges at about 12.5 GPa, coexists with antiferromagnetic order in a narrow pressure range

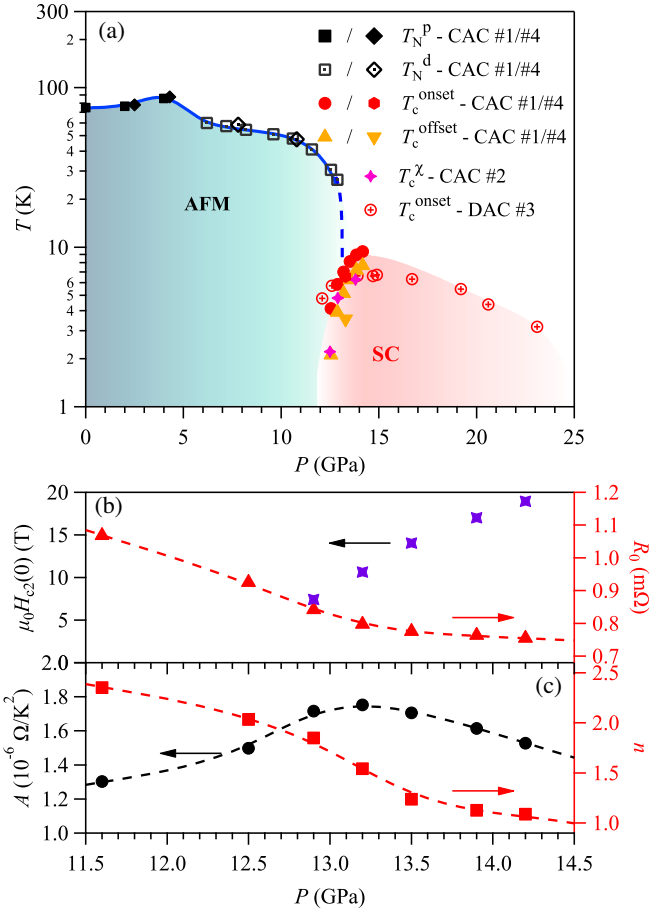

FIG. 4. (a) Temperature-pressure phase diagrams for KMn_6Bi_5. The characteristic temperatures for the antiferromagnetic transition T_N and the superconducting transition T_c^{onset}, T_c^{offset} and T_c^{χ} are determined from the resistance and ac magnetic susceptibility measurement on samples #1 to #4. AFM and SC denote the antiferromagnetic and superconducting phase, respectively. Pressure dependences of (b) $\mu_0 H_{c2}(0)$ and R_0, and (c) the coefficient A and the exponent n.

of 12.5–12.9 GPa, and then increases continuously after the collapse of antiferromagnetic order above P_c. Eventually, a superconducting dome appears on the border of long-range antiferromagnetic order, resembling many unconventional superconducting systems [1–6]. In concomitant with the enhancement of $T_c(P)$ from 12.9 to 14.2 GPa, $\mu_0 H_{c2}(0)$ also increases with pressure as shown in Fig. 4(b).

The close proximity of superconductivity to a magnetic instability suggests that the critical magnetic fluctuations may play an important role in mediating Cooper pairs. To substantiate this point, we analyzed the normal-state resistance just above T_c, which can be fitted by the power law, $R = R_0 + A \times T^n$, where R_0 represents the residual resistance, the coefficient $A(n = 2)$ and the exponent n are associated with the density of states at Fermi level and the inelastic electron scattering, respectively. As shown in Fig. 4(c), the exponent n initially decreases from ~2.0

for Fermi liquid at 12.5 GPa to a minimum ~1.0 for no-Fermi liquid at 14.2 GPa, implying the breakdown of Fermi-liquid state around P_c; the reduction of n is closely related with the collapse of antiferromagnetic order that produces enhanced critical spin fluctuations. Although the enhancement of coefficient A is not significant as typically seen near a magnetic QCP, the broad maximum of A is positively correlated with the evolution of $T_c(P)$. Thus, the observations of non-Fermi-liquid behavior and moderate enhancement of coefficient A near P_c in KMn_6Bi_5 signal the important role of magnetic fluctuations in its transport properties [4–7]. In this regard, pressure-driven quantum phase transition around P_c from the magnetically ordered state to the superconducting state should be a second-order type associated with the continuous suppression of the antiferromagnetic transition.

As mentioned above, the T-P phase diagram of KMn_6Bi_5 featured by the emergence of superconductivity on the border of antiferromagnetic order resembles those of many unconventional superconductors associated with magnetism-medicated pairing mechanism [1–6]. Its unconventional nature is also substantiated by the observations of strange-metal behavior in the normal-state resistance near P_c and an unusually large $\mu_0 H_{c2}(0)$ exceeding the Pauli limit. Previous theoretical calculations in its sister compound $RbMn_6Bi_5$ suggest dominant contributions of Mn-3d orbital electrons to the density of states at Fermi level. If the electronic structures are retained under pressure, KMn_6Bi_5 becomes the first ternary Mn-based superconductor with a relatively high T_c of 9.3 K, which is one order of magnitude higher than that of MnP (~1 K) [7].

The discovery of superconductivity in the *ternary* KMn_6Bi_5 is important for the following reasons: (i) the intriguing crystal structure renders a complex magnetic structure within the inner Mn-cluster column, making it a good candidate to study the geometrically frustrated magnetism and unconventional Cooper pairing; (ii) it proves that T_c of Mn-based superconductors can be raised to the level of 10 K; (iii) the Q1D magnetic materials with enhanced magnetic fluctuations can serve as a new paradigm for finding more Mn-based superconductors, as exemplified in the cases of $A_2Cr_3As_3$ [16–19] and ACr_3As_3 [20,21] (A = K, Rb, Cs, or Na); (iv) in comparison with the binary MnP, the crystal structure and chemical compositions of ternary AMn_6Bi_5 are more flexible and offer more possibilities to explore. For example, one can tune the magnetic and transport properties at AP through chemical substitutions at either A or Bi sites so as to induce superconductivity, e.g., alkaline-earth-doped AMn_6Bi_5, or replacing Bi with Sb/Te in AMn_6Bi_5. On the other hand, whether the infinite $[Mn_6Bi_5]^-$ columns could sever as a new superconducting gene deserves further investigations. Electronic structure and superconducting properties of AMn_6Bi_5 upon varying the A-site cation also deserve in-depth investigations under pressure.

Conclusion.—In summary, we discovered the first ternary Mn-based superconductor KMn_6Bi_5 under high pressure. We found that bulk superconductivity emerges in the pressurized single-crystal KMn_6Bi_5 when its antiferromagnetic order is suppressed by pressure, resulting in a superconducting dome in the vicinity of antiferromagnetic order. The close proximity of superconductivity to a magnetic instability suggests an unconventional paring mechanism. The optimal T_c^{onset} reaches ~9.3 K at 14.2 GPa, and $\mu_0 H_{c2}(0)$ is found to exceed the Pauli paramagnetic limit. The present study can open a new avenue for finding more Mn-based superconductors.

This paper is dedicated to Professor John B. Goodenough on the occasion of his 100th birthday.

This work is supported by the Beijing Natural Science Foundation (Z190008), National Key R&D Program of China (2018YFA0305700, 2021YFA1400200), the National Natural Science Foundation of China (Grants No. 12025408, No. 11874400, No. 11834016, No. 11921004, No. 11888101, No. 12174424), the Strategic Priority Research Program and Key Research Program of Frontier Sciences of CAS (XDB25000000, XDB33000000 and QYZDB-SSW-SLH013), the CAS Interdisciplinary Innovation Team (JCTD-2019-01), Lujiaxi international group funding of K. C. Wong Education Foundation (GJTD-2020-01), and the Users with Excellence Program of Hefei Science Center CAS (2021HSC-UE008). IOP Hundred-Talent Program (Y7K5031X61), and Youth Promotion Association of CAS (2018010). Y. U. acknowledges the support from JSPS KAKENHI (Grant No. JP19H00648).

[*]These authors contributed equally to this work.
[†]Corresponding author.
bswang@iphy.ac.cn
[‡]Corresponding author.
gfchen@iphy.ac.cn
[§]Corresponding author.
jgcheng@iphy.ac.cn

[1] J. G. Bednorz and K. A. Müller, Possible high T_c superconductivity in the Ba-La-Cu-O system, Z. Phys. B Condens. Matter **64**, 189 (1986).
[2] P. A. Lee, N. Nagaosa, and X.-G. Wen, Doping a Mott insulator: Physics of high-temperature superconductivity, Rev. Mod. Phys. **78**, 17 (2006).
[3] Y. Kamihara, H. Hiramatsu, M. Hirano, R. Kawamura, H. Yanagi, T. Kamiya, and H. Hosono, Iron-based layered superconductor: LaOFeP, J. Am. Chem. Soc. **128**, 10012 (2006).
[4] Y. Kamihara, T. Watanabe, M. Hirano, and H. Hosono, Iron-based layered superconductor $La[O_{1-x}F_x]FeAs$ ($x = 0.05 - 0.12$) with $T_c = 26$ K, J. Am. Chem. Soc. **130**, 3296 (2008).
[5] F. Steglich, J. Aarts, C. D. Bredl, W. Lieke, D. Meschede, W. Franz, and H. Schäfer, Superconductivity in the Presence

of Strong Pauli Paramagnetism: $CeCu_2Si_2$, Phys. Rev. Lett. **43**, 1892 (1979).
[6] G. R. Stewart, Heavy-fermion systems, Rev. Mod. Phys. **56**, 755 (1984).
[7] J. G. Cheng, K. Matsubayashi, W. Wu, J. P. Sun, F. K. Lin, J. L. Luo, and Y. Uwatoko, Pressure Induced Superconductivity on the Border of Magnetic Order in MnP, Phys. Rev. Lett. **114**, 117001 (2015).
[8] J. K. Bao, Z. T. Tang, H. J. Jung, J. Y. Liu, Y. Liu, L. Li, Y. K. Li, Z. A. Xu, C. M. Feng, H. Chen, D. Y. Chung, V. P. Dravid, G. H. Cao, and M. G. Kanatzidis, Unique $[Mn_6Bi_5]^-$ nanowires in KMn_6Bi_5: A quasi-one-dimensional antiferromagnetic metal, J. Am. Chem. Soc. **140**, 4391 (2018).
[9] L. Chen, L. Zhao, X. Qiu, Q. Zhang, K. Liu, Q. Lin, and G. Wang, Quasi-one-dimensional structure and possible helical antiferromagnetism of $RbMn_6Bi_5$, Inorg. Chem. **60**, 12941 (2021).
[10] Y. Uwatoko, K. Matsubayashi, T. Matsumoto, N. Aso, M. Nishi, T. Fujiwara, M. Hedo, S. Tabata, K. Takagi, M. Tado, and H. Kagi, Development of palm cubic anvil apparatus for low temperature physics, Rev. High Pres. Sci. Tech. **18**, 230 (2008).
[11] J. G. Cheng, K. Matsubayashi, S. Nagasaki, A. Hisada, T. Hirayama, M. Hedo, H. Kagi, and Y. Uwatoko, Integrated-fin gasket for palm cubic-anvil high pressure apparatus, Rev. Sci. Instrum. **85**, 093907 (2014).
[12] See Supplemental Material at http://link.aps.org/supplemental/10.1103/PhysRevLett.128.187001 for the sample dimensions, the estimated upper critical fields and coherence lengths, the detailed high-pressure resistance data of samples #1, #3, and #4, and the single XRD data of sample #4 before and after high-pressure resistance measurements.
[13] K. Y. Chen, N. N. Wang, Q. W. Yin, Y. H. Gu, K. Jiang, Z. J. Tu, C. S. Gong, Y. Uwatoko, J. P. Sun, H. C. Lei, J. P. Hu, and J. G. Cheng, Double Superconducting Dome and Triple Enhancement of T_c in the Kagome Superconductor CsV_3Sb_5 Under High Pressure, Phys. Rev. Lett. **126**, 247001 (2021).
[14] M. Tinkham, Effect of fluxoid quantization on transitions of superconducting films, Phys. Rev. **129**, 2413 (1963).
[15] A. M. Clogston, Upper Limit for the Critical Field in Hard Superconductors, Phys. Rev. Lett. **9**, 266 (1962).
[16] J.-K. Bao, J.-Y. Liu, C.-W. Ma, Z.-H. Meng, Z.-T. Tang, Y.-L. Sun, H.-F. Zhai, H. Jiang, H. Bai, C.-M. Feng, Z.-A. Xu, and G.-H. Cao, Superconductivity in Quasi-One-Dimensional $K_2Cr_3As_3$ with Significant Electron Correlations, Phys. Rev. X **5**, 011013 (2015).
[17] Z.-T. Tang, J.-K. Bao, Y. Liu, Y.-L. Sun, A. Ablimit, H.-F. Zhai, H. Jiang, C.-M. Feng, Z.-A. Xu, and G.-H. Cao, Unconventional superconductivity in quasi-one-dimensional $Rb_2Cr_3As_3$, Phys. Rev. B **91**, 020506(R) (2015).
[18] Z.-T. Tang, J.-K. Bao, Z. Wang, H. Bai, H. Jiang, Y. Liu, H.-F. Zhai, C.-M. Feng, Z.-A. Xu, and G.-H. Cao, Superconductivity in quasi-one-dimensional $Cs_2Cr_3As_3$ with large interchain distance, Sci. China Mater. **58**, 16 (2015).
[19] Q.-G. Mu, B.-B. Ruan, B.-J. Pan, T. Liu, J. Yu, K. Zhao, G.-F. Chen, and Z.-A. Ren, Ion-exchange synthesis and superconductivity at 8.6 K of $Na_2Cr_3As_3$ with quasi-one-dimensional crystal structure, Phys. Rev. Mater. **2**, 034803 (2018).
[20] Q.-G. Mu, B.-B. Ruan, B.-J. Pan, T. Liu, J. Yu, K. Zhao, G.-F. Chen, and Z.-A. Ren, Superconductivity at 5 K in quasi-one-dimensional Cr-based KCr_3As_3 single crystals, Phys. Rev. B **96**, 140504(R) (2017).
[21] Z.-T. Tang, J.-K. Bao, Y. Liu, H. Bai, H. Jiang, H.-F. Zhai, C.-M. Feng, Z.-A. Xu, and G.-H. Cao, Synthesis, crystal structure and physical properties of quasi-one-dimensional $ACr_3As_3 (A = Rb, Cs)$, Sci. China Mater. **58**, 543 (2015).